Journal of Materials Science and Engineering A 7 (9-10) (2017) 246-257
doi: 10.17265/2161-6213/2017.9-10.003

Bactericidal Action of Silver Nanoparticles Dispersed in Silica Synthesized through the Sol Gel Method

Dolores Silvia Solís Mendiola[1], Ulises Arellano Sánchez[1], Maximiliano Joel Asomoza Palacios[1], Jin An Wang[2], Lifang Chen[2] and Fancisco Javier Tzompantzi Morales[1]

1. Departamento de Química, Universidad Autónoma Metropolitana-Iztapalapa, Av. San Rafael Atlixco No. 186, Iztapalapa, Mexico City 09340, Mexico

2. ESIQIE, Instituto Politécnico Nacional, Col. Zacatenco, Av. Politécnico s/n, Mexico City 07738, Mexico

Abstract: A series of Ag^0 nanoparticle materials supported in SiO_2 were synthesized by the sol-gel method, with contents of 2, 5 and 10% w/w. The fresh samples were calcinated and reduced with H_2 at 500 °C in order to obtain Ag^0. The materials obtained were studied by X-ray diffraction, N_2 physisorption, UV-vis spectroscopy, electronic transmission microscopy and EDS (energy dispersive spectrometer). The antibacterial activity was observed in the deactivation of *E. coli* in its liquid phase, using the plate count method to identify viable CFU (colony forming units). The results show that the materials containing Ag nanoparticles dispersed in SiO_2 increase their bactericidal efficiency on the increase of the content and size of Ag nanoparticles.

Key words: Sol-gel synthesis, Ag-SiO_2, Ag^0 dispersion, bactericidal action, silica matrix**.**

Nomenclature

XAg-SiO_2:	where X represents the 2, 5 and 10% weight/weight of Ag^0
SiO_2:	reference
CF:	colony forming units

Greek letters

λ:	wavelength

1. Introduction

The surge of new strains of bacteria resistant to current antibiotics has become a serious public health problem, therefore, there is a strong incentive to develop new bactericidal agents [1, 2]. It is for this reason that the current research of nanomaterials with bactericidal action will be of great interest. Nanoscience is responsible for the study of nanostructured materials, including their synthesis and application to physical, chemical and biological systems. Bionanoscience is a promising area, which permits the obtaining of knowledge for resolving problems in the areas of medicine, biotechnology and pharmacy [3]. Nanomaterials have received special attention due to their singular electronic, magnetic, optical and catalytic properties. In the area of Biomedicine, there are two relevant characteristics that distinguish them from other materials: (i) due to their size, they can arrive with greater speed and effectiveness to a selected target after being administrated and (ii) the area/volume ratio is greater than in macroscopic materials, which therefore permits modification of their surface with a greater quantity of active molecules, which then offers a greater exposition of the material on the selected target [4]. The application of these materials has been proposed for the treatment of infections commonly

Corresponding author: Ulises Arellano Sánchez, investigator profesor of chemistry department, research fields: (1) photodegradation of organic and biological contaminants by advanced oxidation processes, (2) design, synthesis and characterization of new nanomaterials by the sol-gel method, (3) synthesis and characterization of thin films and photocatalytic nanomaterials, (4) phase oxidation systems liquid and organic, (5) elimination of sulphide compounds by oxidation, (6) multiphase and biphasic reaction systems in continuous reactors, (7) catalytic reactions (oxidative desulfurization technique), (8) elimination of sulfur compounds in petroleum derivatives, (9) synthesis and characterization of biomaterials.

caused by fungi or bacteria [5]. The bacteria are single-cell unicellular prokaryote organisms within the scale of a micrometer. These organisms do not have a nuclear membrane, mitochondria or a true nucleus, and they reproduce through asexual division. They have a cell wall composed of peptidoglycan or murein, which gives form and rigidness to the bacteria. The structure of peptidoglycan is conformed of two sugar derivatives, N-acetyl-glucosamine and N-acetylmuramic acid joined by peptide bonds from a group of amino acids that include L-alanine, D-alanine, D-glutamic, lysine, or diaminopimelic acid. The bacteria have different structures in the membrane, which allow their general classification as gram-negatives or gram-positives [6]. The cell wall structure of the gram-positive bacteria is composed of a thin peptidoglycan layer, with joined teichoic acids. The gram-negative bacteria are composed of a thin peptidoglycan layer and an internal and external cellular membrane, obtaining thereby a more complex cell wall [7, 8]. Currently, with the increase in nanotechnology, materials, which present a noticeable microbicidal, effect when used on a wide variety of microorganisms such as viruses, bacteria and fungi were developed [9]. The microbicidal capacity is related to the nature of the material and certain intrinsic characteristics, like their size and high specific surface area. In the search for new materials, attention has been focused on amorphous SiO_2 due to its porosity and high specific surface area [10]. The pure SiO_2 is chemically inert which limits its application as a catalytic material, so efforts have focused on incorporating into its matrix active phases in the form of metals or oxides to promote acid-base or redox properties [11]. Probably, the most important at the present time is the reuse of the materials, since a high number of applications demand to make the processes more efficient, amorphous SiO_2 is a support that fulfills these demands.

Among the active phases of these materials, those formed by Ag, ZnO, Cu and iron oxides are mentioned. Microbicidal properties of iron oxides present and become evident when they have a nanostructure form, meanwhile the Ag, ZnO and Cu are present and evident in their macroscopic form [9]. Ag nanoparticles show totally different mechanisms of microbicidal action from traditional antibiotics, thereby providing an alternative promissory. The biocidal action and mechanisms that the Ag nanoparticles present on microorganisms have not been completely elucidated [5]. The metallic Ag^0 nanoparticles have been given greater interest due to Ag salts that have been utilized in pharmaceutical preparations such as topical creams. Large application of Ag^0 is due to its low probability of developing resistance to microorganisms in comparison with antibiotics [12]. *E. coli* is representative of the enterobacteriaceae family, which is facultative anaerobic. Some types of *E. coli* can cause illnesses such as hemorrhagic colitis, hemolytic uremic syndrome thrombocytopenic purpura and cause diarrhea. The most dangerous type of *E. coli* causes hemorrhagic diarrhea which can frequently cause kidney malfunction and even death. The suffering of these symptoms generally occurs in children and adults with compromised immune systems [2]. *E. coli* related infections can be acquired by consuming foods which contain the bacteria and ingesting water contaminated with human waste, which causes nausea and vomiting, severe stomach pains and watery or bloody diarrhea. Serious diarrhea related illness is one of the most important public health problems in the world since it affects all age groups. *E. coli* is responsible for approximately 630 million cases of diarrhea worldwide and between 5 and 6 million deaths per year, principally affecting the infant population in developing countries. This work centers on the preparation and characterization of Ag^0 nanoparticles with bactericidal properties, dispersed in a matrix of SiO_2 with a highly specific area. The bactericidal activity of the materials was studied in the deactivation of *E. coli*.

2. Experimental Setup

2.1 Synthesis

The materials were synthesized by the Sol-Gel method from TEOS (tetraethyl orthosilicate) and $AgNO_3$. The method consists of: (1) Mixing 116.8 mL of ethanol and 113.6 mL of TEOS, the solution is stirred over 2 hours; (2) Slowly adding 22.5 mL of $AgNO_3$/deionized water solution previously prepared with 1.7, 4.25 and 8.5 g of $AgNO_3$ in order to obtain materials with 2, 5 and 10% weight/weight respectively, it is stirred for 2 hours, and then adjusting the pH at 6 with HNO_3; (3) The stirring was continued for 24 hours, afterwards it was refluxed at 40 °C for 72 hours, after this time the solvents were evaporated at 40 °C without stirring for the necessary time until the gel was obtained. After the evaporation, the resulting solid is filtered, washed with deionized water and the excess humidity was eliminated by heating in an oven at 60 °C for 48 hours, and was calcinated at 500 °C for 8 hours heating at a speed of 1 °C/min. The materials obtained were reduced in a flux of H_2 at 500 °C. The resulting samples were labeled as XAg-SiO_2 where X represents the 2, 5 and 10% weight/weight of Ag^0, the reference was labeled as SiO_2.

2.2 Characterization

The X-ray diffraction patterns were obtained in a Siemens D500 diffractometer coupled with a tube with copper anode with a Cuk radiation (λ = 1.5406 Å), 35 kV and 20 Ma, selected with a diffracted beam monochromator. The patterns of X-ray diffraction were registered in 2θ between 5 and 70° with a step of 0.02° and a measurement time of 2.67 seconds at each point. The determination of the UV-vis spectra of the materials was obtained in a UV-vis Cary 100 spectrophotometer. The specific area was determined in a Micromeritics equipment ASAP2000, using N_2 as adsorbent at 77 K. The samples were degasified in vacuum at 100 °C for 2 hours and 300 °C during 20 hours, previous to measurement. The TPR technique was carried out with conventional TPD/TPR 2900 machine of Micromeritics, provided with a TCD detector. The procedure consisted of calcination of the material in an air flux from room temperature up to 500 °C, then cooling until room temperature, stabilizing the detector for 1 hour. The measurement was carried out in a flux of 10% hydrogen-helium, heating at 10 °C/min up to 500 °C, H_2 consumption was registered from the thermogram. The images were obtained with a high-resolution microscope, HRTEM Jeol 2100F, using a field emitter as a source of illumination and 200 kV of acceleration, with a resolution of 1.86 Å. It has an EDS detector (energy dispersive X-ray analysis) for elemental analysis.

2.3 Growth Medium

Saline solution: 500 mL of NaCl saline solution was prepared at 0.9%, 9 mL of this solution was then distributed in threaded tubes, and they were sterilized in an autoclave at 121 °C, and 15 lb/in^2 of pressure during 15 minutes. LB (Luria Bertani) growth medium: 10 g/L of casein peptone, 10 g/L sodium chlorine and 5 g/L yeast extract suspended in 800 mL of distilled water, stirred and filled up to 1 L. The pH was adjusted at 7.2±0.2 with sodium hydroxide solution 10 N and sterilized in an autoclave at 121 °C and 15 lb/in^2 of pressure lasting 15 minutes. EMB (eosine methylene blue) agar: 36 g of EMB medium were suspended in 1 L of distilled water and left to sit for 5 minutes to later be heated up to boiling point for 1 or 2 minutes until dissolution. The EMB medium was adjusted at pH 7.2±0.2 with sodium hydroxide solution 10 N and was treated with the same experimental conditions employed for the previous medium (Luria Bertani growth medium).

Preparation of petri dishes: The EMB medium was left to cool until 50 °C and distributed into petri dishes in a sterile area. They were left to solidify to later be incubated during a period of 24 hours.

2.4 Determination of Number of Bacteria

The number of bacteria present in a given volume is determined through the cell plate count technique and by the determination of turbidity. The first technique allows to quantifying the number of viable bacteria (colony forming units CFU), and the second measures the total biomass of the microbial population.

Plaque-count technique: (1) An aliquot of 1 mL is taken in sterile conditions from the medium where the deactivation reaction is carried out. (2) It is diluted in a threaded tube with 9 mL of saline solution, this one being a dilution of 10^{-1} and then stirred. (3) An aliquot of 1 mL is taken from the first tube (10^{-1}) and is taken to a new tube with 9 mL of saline solution, this being the dilution 10^{-2}. (4) Steps 2 and 3 are repeated until a dilution of 10^{-10} is reached. (5) The 0.05 mL of each one of the dilutions is taken, and grown in petri dishes previously prepared with solid EMB medium. (6) The inoculum is dispersed over the entire surface of the agar with the help of a sterile glass handle. (7) It is incubated at 37 °C. (8) The counts of the colony forming units are carried out (CFU/min) at 24, 48 and 72 hours. The dilutions are prepared by duplicate.

2.5 Growth Kinetics

Before carrying out the deactivation experiment, the life cycle of the *E. coli* population was researched. This was carried out by measuring the turbidity with the following procedure: 2 threaded tubes were prepared at the same time as the reactor where the deactivation was carried out with 4.5 and 135 mL of LB medium respectively. Afterwards, in a sterile area, they were inoculated with 0.5 mL and 10 mL of *E. coli* and both incubated at 37 °C. The growth was monitored by spectrophotometer during 6 hours in the threaded tubes in the following manner: (1) the spectrophotometer was calibrated at 580 nm. (2) The previously inoculated tubes were stirred with the help of a vortex. (3) The absorbance was measured at intervals of 1 hour (4) the measurements were carried out until the stationary phase was reached.

2.6 E. coli Deactivation Kinetics

A 250 mL Pyrex beaker glass was used as a reactor, which was placed over a magnetic stirrer. The deactivation reaction was realized at atmospheric pressure with stirring at 37 °C, the reaction was maintained for 1 hour taking aliquots of 1 mL every 30 minutes. The material mass used was 100 mg for every 100 mL of LB medium previously inoculated with *E. coli*. Once it has reached the stationary phase of growth, a sample of 1 mL is taken in sterile reactor conditions and to this sample the plaque-count technique is applied, and this was labeled as Zero Time. Afterwards, the material is placed in the reactor to commence the deactivation. Samples were taken at 30 and 60 minutes and the plaque technique was applied to these, and they were then labeled as Time 1 and 2, respectively. The experiments were realized by duplicate and each point in Figs. 8 and 10 represents the average of the measurements.

3. Experimental Results

3.1 Ag Reduction

Fig. 1 shows the profiles of reduction, at programed temperature (TPR) of H_2 in the samples XAg-SiO_2, two signs of reduction in the interval of 113 to 130 °C and 465 to 485 °C were observed. The peak intensity

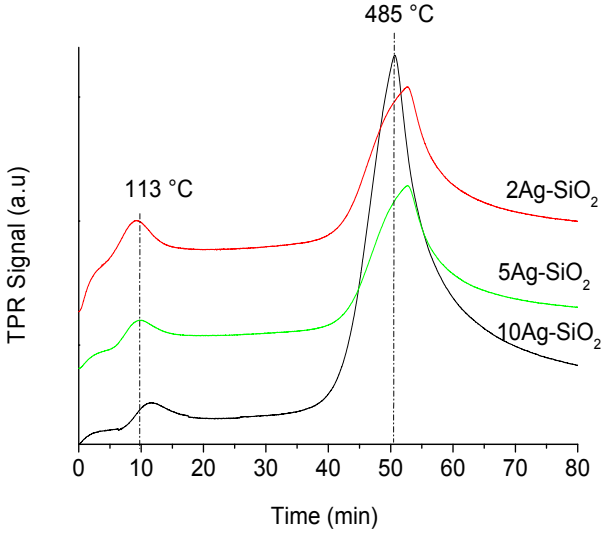

Fig. 1 Reduction thermograms of the materials XAg-SiO_2.

that appears at a lower temperature stays constant on increasing the content of Ag^+, this can be attributed to the reduction of nanocrystals of Ag^+ in the form of Ag_2O that are not agglomerated, and are found highly dispersed in the silica matrix. The Ag^+ does not exchange in the network structure of SiO_2 due to its ionic radio, which is excessively big in comparison with that of Si^{4+}, (Ag^{+1} = 1.26 Å and Si^{4+} = 0.40 Å) and that is why at a lower content of Ag^+ equals greater dispersion in the network structure and less forming of agglomerates of Ag^+ nanoparticles. The highest temperature peak can be attributed to the Ag^+ forming large nanocrystal agglomerates of Ag_2O on the surface of the silicon matrix and the intensity of the greatest temperature peak increases with the content of Ag^+. Reduction at greater temperatures of the large clusters of Ag_2O nanocrystals is attributed to the fact that the Ag is agglomerated and the H_2 has to reduce the agglomeration mass. In the reference material SiO_2, no peak of H_2 consumption was observed.

Table 1 shows the maximum reduction temperatures and the H_2 consumption of the samples of XAg-SiO_2, the H_2 consumption of the first peak is relatively constant and the consumption of the second peak increases in relation to the content of Ag.

3.2 X-ray Diffraction

Fig. 2 shows the patterns of X-ray diffraction of the materials that contain Ag^0 nanoparticles and peaks at 2θ at 38.8, 43.74 and 64.5° are observed, which correspond to plane 111, 002 and 220. No diffraction peak attributable to Ag_2O was detected. The diffraction peaks are attributed to the planes corresponding to the cubic, centered crystalline structure of the Ag^0. The widening of the peaks can be attributed to the very small crystals (nanocrystals). A wide peak centered on 25 °C, above axis 2, corresponding to amorphous SiO_2, was observed.

Table 1 Reduction temperature and hydrogen consumption.

Sample	Maximum temperature (°C)	μmoles H_2/g	Total
	I	II	I
2Ag-SiO_2	129	465	17.7
5Ag-SiO_2	114	485	23.7
10Ag-SiO_2	113	485	24.6

3.3 DRS-UV-vis (Diffuse Reflectance Spectroscopy UV-vis)

Fig. 3 shows the UV-vis spectra of the XAg-SiO_2 materials. It is observed that the reference material SiO_2 presents a band in the form of a shoulder at 200-230 nm that is attributed to the Si-O bonds of SiO_2.

The spectra of the XAg-SiO_2 materials have two adsorption signals at 320 nm and 405 nm, which are attributed to two sizes of spherical nanoparticles of

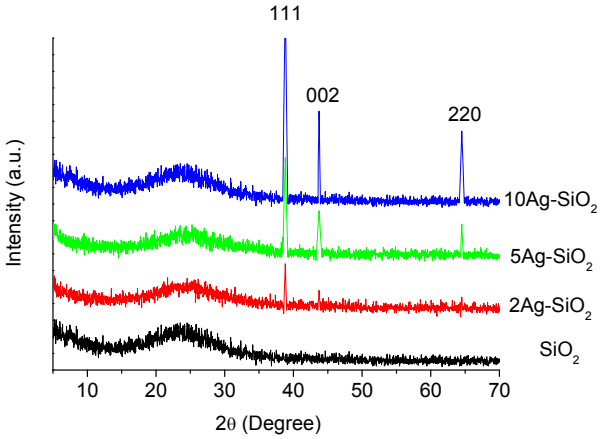

Fig. 2 Diffractograms of the materials XAg-SiO_2.

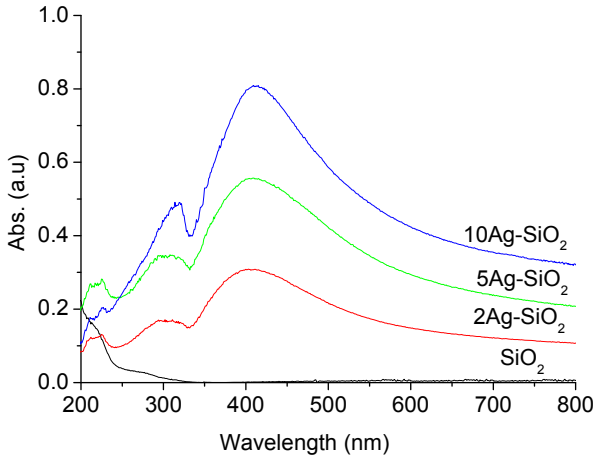

Fig. 3 UV-vis spectroscopy of the materials XAg-SiO_2.

Ag^0 [13]. An increase in absorbance is observed by increasing the content, indicating a higher concentration of nanoparticles of Ag^0 and consequently an increase in grain size [14]. The absorption spectrum of the nanoparticles of Ag^0 presents a sharp and strong signal which is characteristic of so-called plasmons. This absorption consists of the excitation of the electronic oscillations, in response to an electromagnetic field. The optical properties of silver nanoparticles are established by the morphological parameters of the Ag^0 nanoparticles [15]. The plasmon bands have the same position and symmetry indicating that the same morphology of semi-spherical nanoparticles is present independent of the Ag^0 content [15].

3.4 N_2 Physisorption

Fig. 4 shows the adsorption/desorption isotherms and distribution of pores in the materials XAg-SiO_2. The reference material SiO_2 presents a type IV isotherm (IUPAC classification) typical of mesoporous materials [17]. It presents a narrow cycle of hysteresis in a triangular and parallelogram form type H1 that is characteristic of materials that have a very narrow distribution of pores. This corroborates with the pore diameter distribution, which is monomodal, and which indicates an elevated homogeneity in pore size.

The samples that contain Ag^0 conserve the structure of the reference material, since the isotherms of the Ag^0 materials show the same behavior as SiO_2 mesoporous material, presenting a smaller absorption volume and specific area.

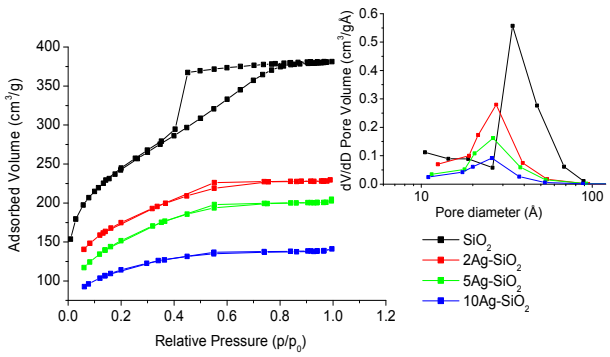

Fig. 4 Adsorption/desorption isotherms and pore distribution.

Table 2 shows textural properties, specific area, volume and pore distribution. It observes that the specific area diminishes and the pore volume increases according to the content of Ag^0, this is attributed to the nanoparticles included in matrix reducing their capacity of absorption, possibly because they partially cover the pores of the SiO_2 matrix. The pore diameter and monomodal distribution are similar in materials with 2, 5 and 10% of Ag, Fig. 4. However, the adsorption volume diminishes when the metal content is increased and this can be attributed to the decreasing of silica ratio on increasing the silver content and some of the silica matrix pores are blocked, thereby occasioning the adsorbed volume to be decreased.

3.5 TEM (Transmission Electron Microscopy)

Fig. 5 shows images of the materials with 2, 5 and 10% of Ag^0 obtained by a TEM. The presence of Ag^0 nanoparticles is observed, which are indicated by arrows. At a lower content of Ag^0 the silver nanoparticles

Table 2 Specific area, volume and pore diameter.

Sample	Specific surface area (m^2)	Vp (cm^3/g)	Dporo (Å)
SiO_2	930	0.496	34
2Ag-SiO_2	624	0.253	27
5Ag-SiO_2	550	0.243	26
10Ag-SiO_2	406	0.150	26

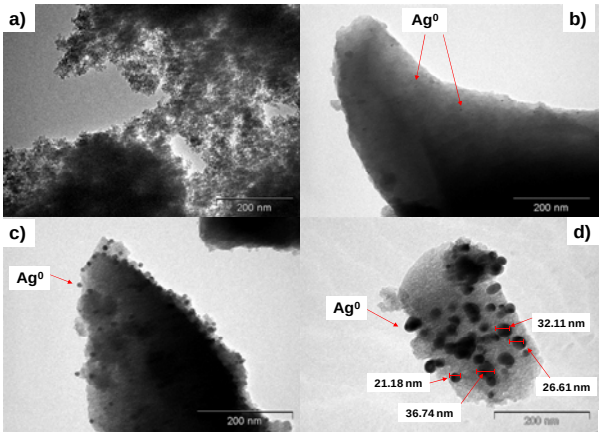

Fig. 5 TEM images, where: (a) SiO_2, (b) 2Ag-SiO_2, (c) 5Ag-SiO_2, (d) 10Ag-SiO_2.

present greater dispersion and smaller diameter.

Fig. 5a corresponds to the porous silica matrix without Ag^0, Figs. 5b-5d correspond to the samples with 2, 5 and 10% of Ag^0, in them it can be appreciated that the Ag^0 dispersed nanoparticles, increase their average diameter to 2 nm, 6 nm and 25 nm respectively. In all cases, the Ag^0 nanoparticles are highly dispersed in the amorphous SiO_2 matrix.

Fig. 6 shows the TEM images and EDS analysis of the materials SiO_2, 2Ag-SiO_2, 5Ag-SiO_2, and 10Ag-SiO_2, it is observed that the SiO_2 is covered by nanoparticles of Ag^0 that increase its size as the Ag content increases. The EDS analysis of the material SiO_2 presents intense peaks attributed to Si kα and O kα indicating the presence of SiO_2. The EDS analysis of the materials 2Ag-SiO_2, 5Ag-SiO_2, and 10Ag-SiO_2 present signals attributed to the SiO_2 that decreases with the increase of the Ag^0 content. The composition of the nanoparticles is primarily Ag^0 as indicated by the Ag Lα signal. The Ag^0 nanoparticles are found on the surface, this is attributed to the fact that Ag^{1+} cannot be incorporated in the SiO_2 network because it has a higher ionic radius than Si^{4+} (Ag^{1+} = 1.26 Å and Si^{4+} = 0.40 Å).

Fig. 7 shows the chemical mapping of elements detected by EDS of materials 2Ag-SiO_2, 5Ag-SiO_2 and 10Ag-SiO_2, represented by green, blue and red pixels for Okα, Sikα and AgLα respectively. It is observed that the catalyst 2Ag-SiO_2 presents a high distribution of the nanoparticles of Ag^0. In the materials 5Ag-SiO_2 and 10Ag-SiO_2, the concentration of the Ag^0 nanoparticles accumulates in small areas forming Ag^0 nanoparticle agglomerates, increasing the diameter of the nanoparticles. Larger diameter nanoparticles are formed by clusters of Ag^0 nanoparticles.

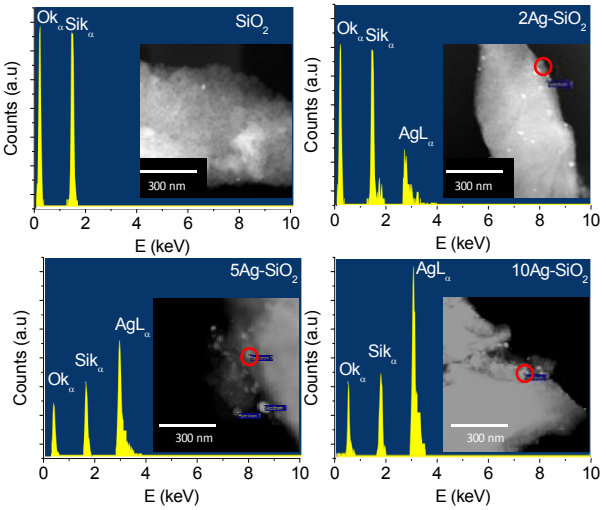

Fig. 6 EDS images of the materials SiO_2, XAg-SiO_2.

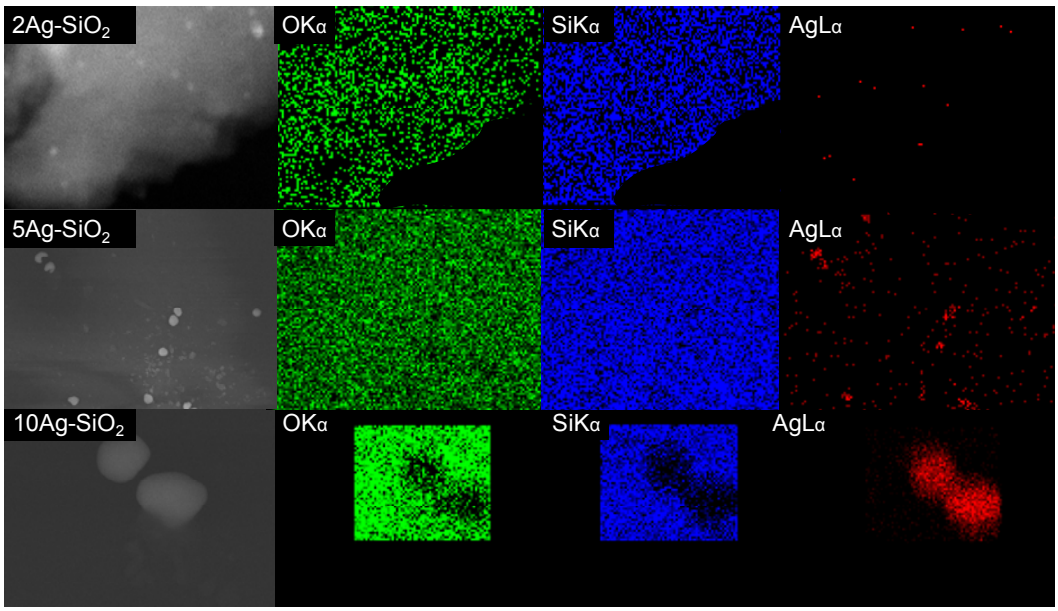

Fig. 7 Elemental chemical mapping of the materials 2Ag-SiO_2, 5Ag-SiO_2 and 10Ag-SiO_2.

3.6 Deactivation of E. Coli

Fig. 8 shows the curve of growth of *E. coli* and it observes the phase of exponential growth with duration of 4 hours attributed to the division of the *E. coli* every 30 minutes in the LB medium at a constant speed. At the end of the exponential phase, the growth speed stops and the stationary phase commences, this can be attributed to the termination of nutrients and the accumulation of metabolism toxic products. A latency phase does not exist, due to the *E. coli* coming from an identical medium and a young culture, and because of this they do not require an adaptation period. In the stationary phase the number of viable *E. coli* stays constant which permits to realize the deactivation experiments that consistently eliminate whichever form of reproduction (a microorganism which does not reproduce is dead). The stationary phase permits to always start with the same population number of *E. coli*. The growth kinetics of the strain of *E. coli* was carried out before each deactivation experiment during 8 hours. The stationary phase reaches an average total biomass concentration of microbial population of 2.50×10^8 CFU/mL (0.525 nm) over a period of 4 hours.

The box in Fig. 8 presents the deactivation kinetics of *E. coli* realized during the stationary phase with the sample 5Ag-SiO_2, the deactivation kinetics of *E. coli* obtained with 2 and 10% of Ag^0 both present a similar tendency. The recount of viable colonies was realized through the plaque-count technique with EMB medium due to the fact that it only identifies viable *E. coli* after the deactivation reaction. Each viable *E. coli* has a place in the formation of a colony after the incubation giving a metallic green color. The number of colonies showing the results in CFU mL^{-1} (colony forming units by mL) was counted.

Fig. 9 presents the viable colonies of *E. coli* in EMB medium before and after the deactivation of the sample 10Ag-SiO_2 in Fig. 9a that corresponds to zero time, where the greatest number of viable colonies of *E. coli* is found. Figs. 9b and 9c correspond to 30 minutes of exposition to the sample 10Ag-SiO_2 and at 60 minutes, respectively, and they observe the inhibition of the colonies of *E. coli* in time function, due to the diminution of viable colonies at 30 minutes and their total deactivation at 60 minutes. These results show the activity of the catalysts that contain Ag^0 as a microbicide agent. The *E. coli* colonies present the characteristic metallic green color.

Fig. 10 indicates the percentage of the number of CFU/mL *E. coli* viable with respect to the exposure time with reference to SiO_2 and the samples with 2, 5 and 10% of Ag^0 content. The diminution of the UFC/mL due to the effect of the Ag^0 nanoparticles dispersed in the samples is notable. The recount shows that 18, 10 and 5% of the *E. coli* manage to survive when exposed for 30 minutes to the samples 2Ag-SiO_2, 5Ag-SiO_2, 10Ag-SiO_2, respectively. These results show that Ag^0 nanoparticles dispersed in SiO_2 are

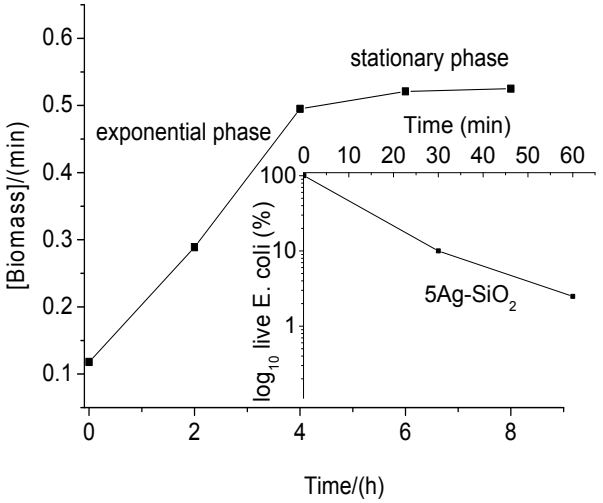

Fig. 8 Growth kinetics of *E. coli* in LB medium.

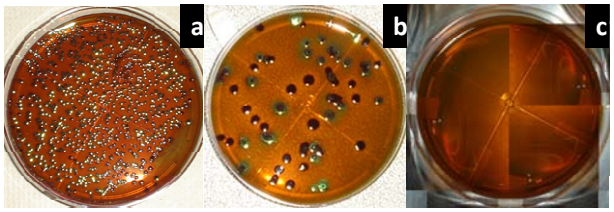

Fig. 9 Viable *E. coli* bacteria in EMB medium, (a) *E. coli* at zero time, (b) *E. coli* at 30 minutes, (c) *E. coli* at 60 minutes.

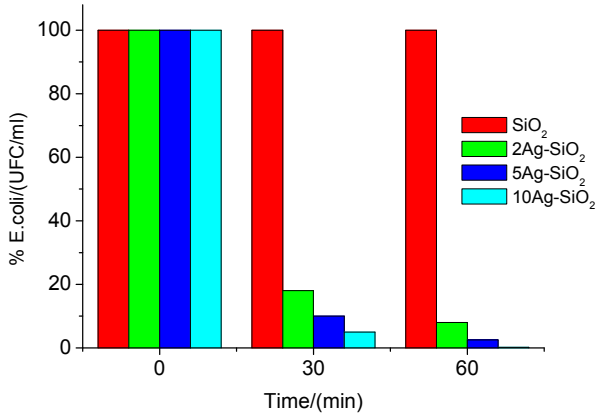

Fig. 10 Number percentage of CFU/mL of viable *E. coli* with respect to exposition time with materials that contain Ag^0.

capable of diminishing the viability of the bacteria from a culture with an elevated initial concentration (2.50×10^8 CFU/mL).

At 60 minutes 8, 2.5 and 0% of the *E. coli* survived, with the catalysts 2Ag-SiO_2, 5Ag-SiO_2, 10Ag-SiO_2 respectively. The silica matrix without Ag^0 does not present bactericidal activity.

Fig. 11 shows the ratio between the dimensions and physical characteristics that exist between the *E. coli* and samples of Ag^0 dispersed in silica. In this study, a strong bactericide effect has been observed when the Ag^0 nanoparticles possess a diameter between 6-25 nm. *E. coli* measures 2 μm in length and has a diameter of 0.5 μm (2,000 × 500 nm) and due to this, it can stick to the surface of large and small particles within the silica matrix with dispersed and exposed nanospheres of Ag^0, as they appear in the images of TEM in Fig. 5.

When Ag^0 is in an aqueous or humid medium it oxidizes forming Ag^+ ions that react with sulphydryl groups of biomacromolecules and with phosphorosulphate compounds like the DNA, inactivating the *E. coli* [18-20].

The bactericidal effect of the Ag^0 nanoparticles has been known for a long time, but the mechanism of action is followed without knowledge in its totality. A bactericidal action mechanism is proposed for the samples XAg-SiO_2 considering the reported studies in the bibliography [2, 17, 21].

In Fig. 12 the mechanism of *E. coli* deactivation with the materials XAg-SiO_2, is presented. The deactivation consists of breaking the cellular membrane and/or phagocytosis of the material with nanoparticles of Ag^0 dispersed in a silica matrix. These two mechanisms consist of the following steps: (1) Sticking of the *E. coli* on the materials surface through charge differences. (2) Breaking *E. coli* cellular membrane modifying its permeability and respiration. (3) Inclusion of the bactericidal material XAg-SiO_2 through the mechanism of phagocytosis to the interior of the *E. coli*. (4) Reaction of the Ag^0 nanospheres with the organelles and DNA. (5) Decomposition of the organic material that composes

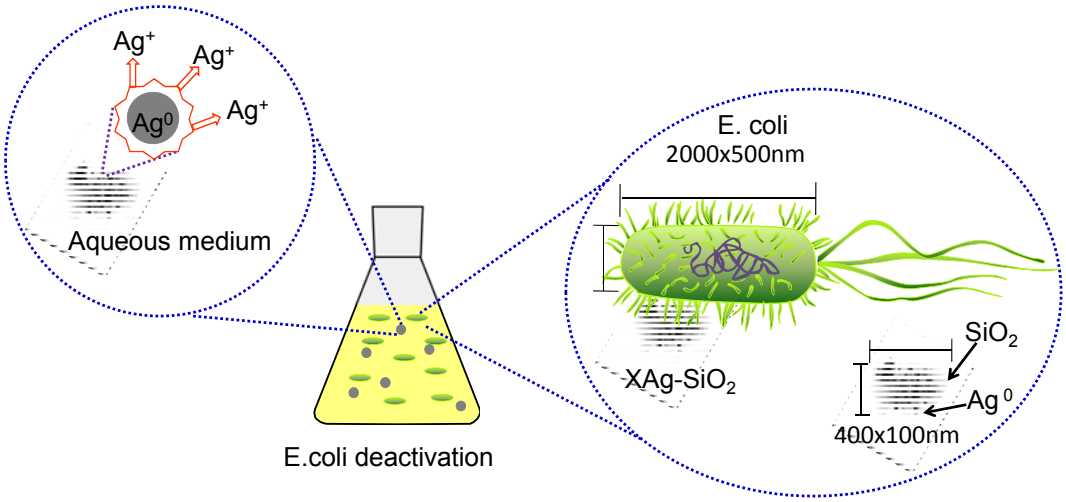

Fig. 11 Intersection between *E. coli* and XAg-SiO_2 materials.

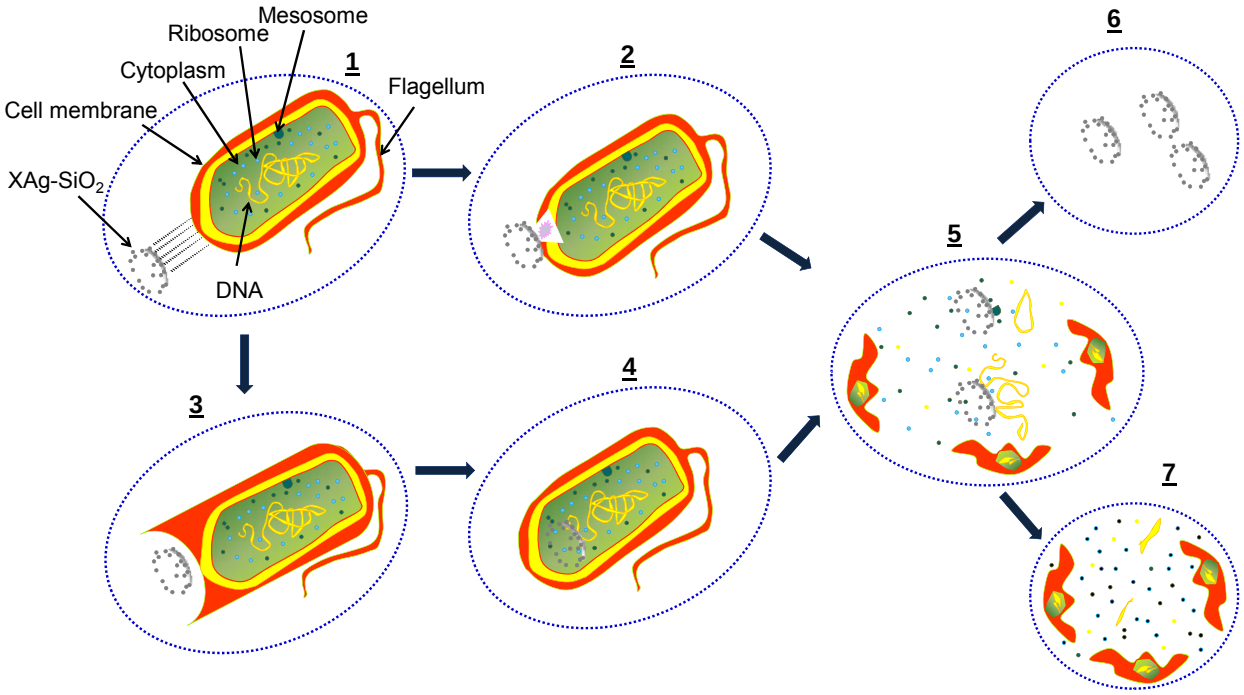

Fig. 12 Deactivation mechanism of *E. coli* with XAg-SiO_2 materials.

the *E. coli*. (6) Separation of the Ag^0 nanospheres dispersed on the silica of the organic material that forms the *E. coli*. (7) Elimination of the compounds from the degradation of the *E. coli*.

In the deactivation route that follows steps 1, 2, 5, 6 and 7 the particles of the samples XAg-SiO_2 do not enter the interior of the *E. coli* due to their size or speed of anti-bacterial action, which therefore destroy the external cellular membrane, since it interacts with the proteins of the membrane, generating pores, causing as a consequence the collapse of the membrane potential, disconnecting the respiratory chain and transport of electrons. This generates oxidative stress which causes death, leaving exposed the material that composes the *E. coli*. The interaction of the biological molecules like DNA, RNA and organelles is not discarded after the destruction of the external membrane, complementing the anti-bacterial action [2, 17].

In the deactivation route that follows steps 1, 3, 4, 5, 6 and 7 the XAg-SiO_2 particle samples surround the *E. coli* cellular membrane through the phagocytosis mechanism, reacting internally with the organelles and genetic material, inhibiting the metabolism and energy production and deactivating the *E. coli*. At the end of the deactivation reaction, by either of the two examined routes, the bactericidal materials can be recovered and reused since the Ag^0 nanospheres are found anchored to the silica matrix [21].

The antimicrobial properties of Ag^0 are already known, since it reacts with the aqueous media, skin humidity and fluid in injuries, which ionizes it. Ionized Ag^0 is highly reactive, since it joins to tissue proteins and provokes structural change in the bacteria cellular wall and cellular membrane which causes distortion and death of the cell. Ag^0 also joins to bacterial DNA and RNA and denaturalizes them, inhibiting the replication of *E. coli*. For this reason, materials with Ag^0 in active phase can be applied in a variety of fields such as medicine. It is not simple to carry out a comparative analysis of bibliographical data, as bactericidal action depends on an ample variety of factors, among these the following can be mentioned: size, nanoparticle form, superficial charge and concentration. The antimicrobial activity of the studied materials can be attributed to the interaction

between the bacteria and the dimensions of the Ag^0 nanoparticles contained in the amorphous silica matrix. The reusable, bactericidal materials XAg-SiO_2 are especially promising when taking into account the variety of bacterial strains resistant to the environment and antibiotics.

4. Conclusions

The process of Sol-Gel synthesis permitted the nanoparticles of Ag^0 to anchor and disperse in the amorphous silica matrix, which means that they can be reutilized in an indefinite number of processes without loss or dilution of the active phase. The results indicate that the bactericidal properties depend on the proportion of Ag^0, 2, 5 and 10% w/w, of the dispersion in the silica matrix and of the average diameter of formed nanoparticles, 2 nm, 6 nm and 25 nm.

The Ag^0 nanoparticles work when they bond to the surface of the cellular membrane of the *E. coli*, changing its basic functions like its permeability and respiration, causing its death. The bactericidal properties that the studied materials XAg-SiO_2 present, are of interest in diverse application fields of, although their mechanism of action continues to be a very active line of research. The bactericidal activity presented by the material XAg-SiO_2 is directly related to the oxidation of Ag^0 present in an aqueous and humid environment.

Acknowledgments

We give our thanks and acknowledgements to Escuela Superior de Ingeniería e Industrias Extractivas (ESIQIE) of IPN (The Superior School of Engineering and Extractive Industries, National Polytechnic Institute), to the department of Catalysis at UAM-I, to Dr. Florina Ramírez from the Department of Biotechnology at UAM-I, to Dr. Patricia Castillo, responsible for the Electronic Microscopy laboratory of the Central Laboratory of UAM-I and the National Council for Science and Technology (CONACYT) for the support received for the realization of the present investigation.

References

[1] Kyriacou, S. V., Brownlow, W. J., and Xu, X-H. N. 2004. "Using Nanoparticle Optics Assay for Direct Observation of the Function of Antimicrobial Agents in Single Live Bacterial Cells." *Biochemistry* 43: 140-7.

[2] Sondi, I., and Salopek-Sondi, B. 2004. "Silver Nanoparticles as Antimicrobial Agent: A Case Study on *E. coli* as a Model for Gram-Negative Bacteria." *Journal of Colloid and Interface Science* 275: 177-82.

[3] Seil, J. T., and Webster, T. J. 2012. "Antimicrobial Applications of Nanotechnology: Methods and Literature." *International Journal of Nanomedicine* 7: 2767-81.

[4] Caruthers, S. D., Wickline, S. A., and Lanza, G. M. 2007. "Nanotechnological Applications in Medicine." *Current Opinion in Biotechnology* 18: 26-30.

[5] Hajipour, M. J., Fromm, K. M., AkbarAshkarran, A., Jimenez de Aberasturi, D., Larramendi, I. R. D., Rojo, T., Serpooshan, V., Parak, W. J., and Mahmoudi, M. 2013. "Antibacterial Properties of Nanoparticles." *Trends in Biotechnology* 31: 61-2.

[6] Murray, R. G. E., Steed, P., and Elson, H. E. 1965. "The Location of the Mucopeptide in Sections of the Cell Wall of Escherichia Coli and Other Gram-Negative Bacteria." *Canadian Journal of Microbiology* 11: 547-60.

[7] Costerton, W., Veeh, R., Shirtliff, M., Pasmore, M., Post, C., and Ehrlich, G. 2003. "The Application of Biofilm Science to the Study and Control of Chronic Bacterial Infections." *The Journal of Clinical Investigation* 112: 1466-77.

[8] Shockman, G. D., and Barret, J. F. 1983. "Role of Proton Motive Force in Sensory Transduction in Bacteria." *Annual Review of Microbiology* 37: 501-73.

[9] Barnea Y., Weiss, J., and Gur, E. 2009. "A Review of the Applications of the Hydrofiber Dressing With Silver (Aquacel Ag®) in Wound Care." *International Journal of Nanomedicine* 6: 21-7.

[10] Kang, J., Li, Y., Chen, Y., Wang, A., Yue, B., Qu, Y., Zhao, Y., and Chu, H. 2015. "Core–Shell Ag@Sio2 Nanoparticles of Different Silica Shell Thicknesses: Preparation and Their Effects on Photoluminescence of Lanthanide Complexes." *Materials Research Bulletin* 71: 116-21.

[11] Pinho, L., Rojas M., and Mosquera M. J. 2015. "Ag-SiO_2-TiO_2 Nanocomposite Coatings with Enhanced Photoactivity for Self-cleaning Application on Building Materials." *Applied Catalysis B: Environmental* 78: 144-54.

[12] Castellano, J. J., Shafii, S. M., Ko, F., Donate, G., Wright,

T. E., Mannari, R. J., Payne, W. G., Smith, D. J., and Robson, M. C. 2007. "Comparative Evaluation of Silver-Containing Antimicrobial Dressings and Drugs." *International Wound Journal* 4: 114-22.

[13] Peña, O., and Pal, U. 2010. "Geometrical Tunability of Linear Optical Response of Silica-Gold Double Concentric Nanoshells." *Journal of Physical Chemistry* 114 (10): 4414-7.

[14] Chen, M., Feng, Y. G., Wang, X., Li, T. C., Zhang, J. Y., and Qian, D. J. 2007. "Nanopartículas de plata tapadas por oleilamina: formación, crecimiento and autoorganización." *Langmuir* 23: 5296-304.

[15] An, W., Zhu, T., and Zhu, Q. 2014. "Numerical Investigation of Radiative Properties and Surface Plasmon Resonance of Silver Nanorod Dimers on a Substrate." *Journal of Quantitative Spectroscopy and Radiative Transfer* 132: 28-35.

[16] Choi, H., Bae, J. H., Kim, D. H., Park, Y. K., and Jeon, J. K. 2013. "Butanol Dehydration over V2O5-TiO2/MCM-41 Catalysts Prepared via Liquid Phase, Atomic Layer Deposition." *Materials* 6: 1718-29.

[17] Mirzajani, F., Ghassempour, A., Aliahmadi, A., and Esmaeili, M. A. 2011. "Antibacterial Effect of Silver Nanoparticles on Staphylococcus Aureus." *Research in Microbiology* 162: 542-9.

[18] Guzman, M., Dille, J., and Godet, S. 2011. "Synthesis and Antibacterial Activity of Silver Nanoparticles against Gram Positive and Gram Negative Bacteria." *Nanomedicine: Nanotechnology, Biology and Medicine* 8: 37-45.

[19] Sharma, V. K., Yngard, R. A., and Lin, Y. 2009. "Silver Nanoparticles: Green Synthesis and Their Antimicrobial Activities." *Advances in Colloid and Interface Science* 145: 83-96.

[20] Le, A. T., Tam, L. T., Tam, P. D., Huy, P. T., Huy, T. Q., and Hieu, N. V. 2010. "Synthesis of Oleic Acid-Stabilized Silver Nanoparticles and Analysis of Their Antibacterial Activity." *Materials Science and Engineering: C* 30: 910-6.

[21] Hwang, E. T., Lee, J. H., Chae, Y. J., Kim, Y. S., Kim, B. C., Sang, B. I., and Gu, M. B. 2008. "Analysis of the Toxic Mode of Action of Silver Nanoparticles Using Stress-Specific Bioluminescent Bacteria." *Small* 4: 746-50.